Metal Nitride Cluster Fullerene $M_3N@C_{80}$ (M = Y, Sc) Based Dyads: Synthesis, and Electrochemical, Theoretical and Photophysical Studies

Julio R. Pinzón,[a] Claudia M. Cardona,[a, b] Maria Ángeles Herranz,[c] Marta E. Plonska-Brzezinska,[a, d] Amit Palkar,[a] Andreas J. Athans,[a] Nazario Martín,*[c] Antonio Rodríguez-Fortea,[e] Josep M. Poblet,*[e] Giovanni Bottari,[f] Tomás Torres,*[f] S. Shankara Gayathri,[g] Dirk M. Guldi,*[g] and Luis Echegoyen*[a]

Abstract: The first pyrrolidine and cyclopropane derivatives of the trimetallic nitride templated (TNT) endohedral metallofullerenes I_h-$Sc_3N@C_{80}$ and I_h-$Y_3N@C_{80}$ connected to an electron-donor unit (i.e., tetrathiafulvalene, phthalocyanine or ferrocene) were successfully prepared by 1,3-dipolar cycloaddition reactions of azomethine ylides and Bingel–Hirsch-type reactions. Electrochemical studies confirmed the formation of the [6,6] regioisomers for the $Y_3N@C_{80}$-based dyads and the [5,6] regioisomers in the case of $Sc_3N@C_{80}$-based dyads. Similar to other TNT endohedral metallofullerene systems previously synthesized, irreversible reductive behavior was observed for the [6,6]-$Y_3N@C_{80}$-based dyads, whereas the [5,6]-$Sc_3N@C_{80}$-based dyads exhibited reversible reductive electrochemistry. Density functional calculations were also carried out on these dyads confirming the importance of these structures as electron transfer model systems. Furthermore, photophysical investigations on a ferrocenyl–$Sc_3N@C_{80}$-fulleropyrrolidine dyad demonstrated the existence of a photoinduced electron-transfer process that yields a radical ion pair with a lifetime three times longer than that obtained for the analogous C_{60} dyad.

Keywords: donor–acceptor dyads · electrochemistry · fullerenes · metal–nitride clusters · photophysics

[a] J. R. Pinzón, Dr. C. M. Cardona, Dr. M. E. Plonska-Brzezinska, A. Palkar, Dr. A. J. Athans, Prof. Dr. L. Echegoyen
Department of Chemistry, Clemson University
219 Hunter Laboratories, Clemson, SC 29634 (USA)
Fax: (+1) 864-656-6613
E-mail: luis@clemson.edu

[b] Dr. C. M. Cardona
Luna Innovations, Inc., Nanoworks Division
521 Bridge Street, Danville, Virginia 24541 (USA)

[c] Dr. M. Á. Herranz, Prof. Dr. N. Martín
Departamento de Química Orgánica I
Facultad de Química, Universidad Complutense
28040 Madrid (Spain)
Fax: (+34) 91-394-4103
E-mail: nazmar@quim.ucm.es

[d] Dr. M. E. Plonska-Brzezinska
Institute of Chemistry, University of Bialystok
Hurtowa 1, 15-399 Bialystok (Poland)

[e] Dr. A. Rodríguez-Fortea, Prof. Dr. J. M. Poblet
Departament de Química Física i Inorgànica
Universitat Rovira i Virgili, c/Marcel·lí Domingo s/n

Campus Sescelades, 43007 Tarragona (Spain)
Fax: (+34) 977-559-563
E-mail: josepmaria.poblet@urv.cat

[f] Dr. G. Bottari, Prof. Dr. T. Torres
Departamento de Química Orgánica
Universidad Autónoma de Madrid, 28049 Madrid (Spain)
Fax: (+34) 91-497-3966
E-mail: tomas.torres@uam.es

[g] Dr. S. S. Gayathri, Prof. Dr. D. M. Guldi
Friedrich-Alexander-Universität Erlangen–Nürnberg
Department of Chemistry and Pharmacy & Interdisciplinary Center for Molecular Materials (ICMM)
Egerlandstrasse 3, 91058 Erlangen (Germany)
Fax: (+49) 9131-852-8307
E-mail: dirk.guldi@chemie.uni-erlangen.de

Supporting information for this article is available on the WWW under http://dx.doi.org/10.1002/chem.200801559.

Introduction

Carbon nanostructures such as fullerenes[1,2] and carbon nanotubes (CNTs)[3] represent a fascinating class of materials which are attracting considerable attention due to their potential technological applications, including those in electronic and optoelectronic devices.[1] More recently, a wide variety of new carbon nanostructures, including endohedral fullerenes, have emerged as new and exciting carbon-containing materials whose chemical and physical properties are currently being explored.[4] Among the endohedral fullerenes,[5] the trimetallic nitride templated (TNT) endohedral metallofullerenes—carbon cages that encapsulate trimetallic nitride clusters—have been the focus of great interest since their first synthesis in 1999 by the process developed by Dorn and co-workers.[6] This method has allowed the preparation of TNT endohedral metallofullerenes in high yields. The stabilization of a large variety of endohedral carbon cages, including different isomeric structures or compounds that violate the isolated pentagon rule has been realized, simply by the judicious choice of the trapped metal atoms.[7] In addition, due to their interesting physical properties TNT endohedral metallofullerenes have been investigated for potential applications in the fields of biomedicine and nanomaterials sciences.[8]

Derivatization of these fullerene species is essential to construct novel organo-metallofullerene materials for a variety of future applications. To date, however, reports on the exohedral derivatization of TNT endohedral metallofullerenes are scarce and only a few types of reactions (Diels–Alder,[9] 1,3-dipolar cycloaddition of azomethine ylides,[10] Bingel–Hirsch-type,[11] disilirane addition,[12] radical trifluoromethylation[13] and malonate free radicals[14]) have been reported. The experimental and theoretical studies carried out on these TNT endohedral fullerenes suggest that the chemical reactivity and regioselectivity observed are a consequence of several parameters such as the nature of the encapsulated metal cluster, the carbon cage size, and the symmetry of the endohedral fullerene itself.

A fundamental aspect of TNT endohedral metallofullerenes, which yet awaits exploration, is their possible application in electron donor–acceptor (D–A) systems.[15] Although C_{60} fullerene and higher homologue structures have been extensively incorporated into D–A systems due to their low reorganization energies in charge-transfer processes, as well as their significant electron-mobility features, acting as excellent electron acceptors,[16] only one example of the TNT endohedral fullerenes has ever been explored in this context.[17] In addition, TNT endohedral metallofullerenes possess larger absorptive coefficients than C_{60} in the visible region of the electromagnetic spectrum and a low HOMO–LUMO energy gap, while preserving a remarkable electron accepting ability, similar to that of C_{60}.[8]

In the present work, a series of $M_3N@C_{80}$ (M = Y, Sc) based D–A dyads have been synthesized via 1,3-dipolar cycloaddition reactions of azomethine ylides or Bingel–Hirsch-type reactions. Three different types of donor moieties have been considered in our investigations: i) ferrocene (Fc) derivatives,[18] ii) extended tetrathiafulvalene (exTTF) derivatives,[16e, 19] which exhibit strong stabilization upon oxidation as they gain aromaticity and planarity in the process, thus stabilizing the photolytically generated radical ion pairs in D–A systems and; iii) phthalocyanine (Pcs) derivatives, which are aromatic macrocycles possessing extinction coefficients as high as $200\,000\,M^{-1}\,cm^{-1}$ in the 700 nm range.[20] The chemical reactivity investigations of the I_h-$Sc_3N@C_{80}$ and I_h-$Y_3N@C_{80}$ cages towards the construction of D–A systems were complemented with electrochemical, theoretical, and photophysical studies.

Results and Discussion

Synthesis: The first synthetic strategy pursued for the preparation of $M_3N@C_{80}$-based dyads (M = Y, Sc) was based on the 1,3-dipolar cycloaddition reaction of azomethine ylides, to give rise to a pyrrolidine adduct on the endohedral fullerene moiety (Scheme 1).[21] Cycloaddition reactions of azomethine ylides on endohedral metallofullerenes have been reported, showing different selectivity depending on the metal cluster.[10] Two types of C−C double bonds are available on the $M_3N@C_{80}$ cage (M = Y, Sc) for the reaction with the in situ generated azomethine ylide: the C−C double bonds between two hexagonal rings ([6,6]-junctions) and those between pentagonal and hexagonal rings ([5,6]-junctions). When the fullerene inner metal cluster was Sc_3N, the only product detected was the adduct at a [5,6]-junction. On the other hand, the 1,3-dipolar cycloaddition reaction occurred at a [6,6]-junction for the $Y_3N@C_{80}$. The $Y_3N@C_{80}$ [6,6]-monoadducts proved to be the kinetic products, and they underwent rearrangement to the thermodynamically more stable $Y_3N@C_{80}$ [5,6]-monoadducts upon heating.[22] Recently, both the [6,6] and [5,6]pyrrolidine monoadducts of $Sc_3N@C_{80}$ were isolated when an N-trityl azomethine ylide was employed instead of the N-methyl or N-ethyl analogues.[10e] These experimental results, as well as recent computational studies by Poblet and Echegoyen,[23] seem to indicate that after thermalization of the kinetically favored product, a pirouette-kind of mechanism gives rise to the [5,6]-monoadduct that is thermodynamically preferred. The rate of this rearrangement depends on the internal cluster and on the pyrrolidine addend.

The reactivity of the TNT species proved to be very different to that of empty cage fullerenes and thus the synthetic protocol required adjustments to prepare the desired TNT dyads. An initial attempt to prepare a Pc-substituted pyrrolidine-containing $Sc_3N@C_{80}$ dyad following the procedures optimized for other $Sc_3N@C_{80}$ pyrrolidines[10a,b] was not very effective and only traces of the Pc dyad were obtained after heating for 50 min at 120°C (Figure S1). Similar attempts to prepare the Pc-substituted $Y_3N@C_{80}$ dyad **3** provided some insight into the actual reaction path. In this case the reaction was allowed to go for 5 h and a side product was isolated which did not contain the Pc unit. In fact, fur-

CHEMISTRY
A EUROPEAN JOURNAL

L. Echegoyen, D. M. Guldi, T. Torres, J. M. Poblet, N. Martín et al.
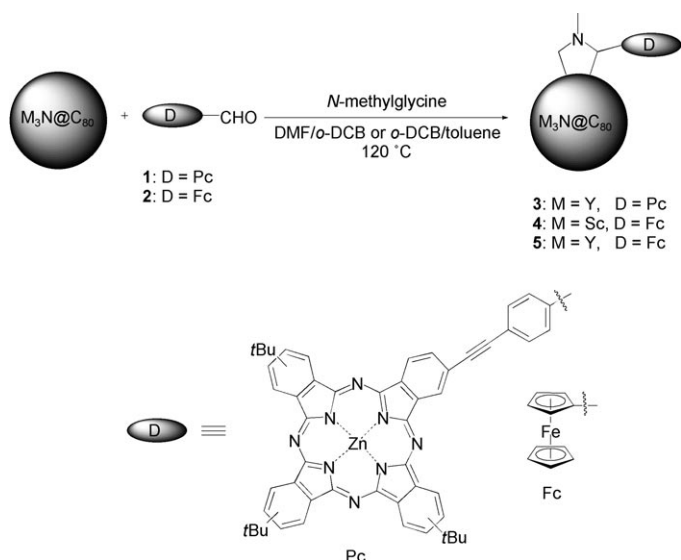
Scheme 1. Synthesis of pyrrolidine-based TNT endohedral metallofullerenes substituted with different donor-bearing aldehydes.

ther characterization of this product revealed it to be the N-methylpyrrolidine derivative which had been previously prepared with N-methylglycine and formaldehyde.[10c] If instead of N-methylglycine, N-ethylglycine was employed the reaction gave similar results; in this case the isolated product was the N-ethylpyrrolidine. Such results seem to indicate that the 1,3-dipolar cycloaddition of the azomethine ylide formed with the aldehyde employed is *not* the only reaction taking place (Figure S2). In fact, the N-methylglycine or N-ethylglycine adds to the carbon sphere in a competitive fashion probably through an electron transfer/radical mechanism giving rise to the pyrrolidine species. Similar reactions have been previously observed with C_{60}[24] and with $Gd@C_{82}$.[25] Based on the proposed mechanism for the formation of the azomethine ylide, removal of any traces of water and a more polar solvent was expected to enhance the formation of the desired ylide. Therefore, synthesis of TNT endohedral pyrrolidino-metallofullerene **3** was carried out by heating a dimethylformamide (DMF)/molecular sieves/*ortho*-dichlorobenzene (o-DCB) mixture containing $Y_3N@C_{80}$ (1 equiv), aldehyde **1**[26] (7–8 equiv) and N-methylglycine (4–7 equiv) at 120 °C. Monoadduct **3** was isolated after silica gel column chromatography using CS_2 as eluent and subsequently purified by HPLC (Figure S3 and S4). The HPLC trace of the crude reaction product of **3** (Figure S3) clearly shows traces of the N-methylpyrrolidine adduct, even when the amounts of N-methylglycine were reduced, which suggests the fact that the modifications in the synthetic procedure enhance the yield of the desired dyad, but it did not completely suppress the side reaction of the TNT species with the glycine. In the matrix assisted laser desorption ionization time-of-flight (MALDI-TOF) mass spectrum of the monoadduct, only the m/z peaks at 901 and 1241 are observed, which correspond respectively, to the pyrrolidino–Pc addend and to the $Y_3N@C_{80}$ cage (Figure S4).

Unfortunately, Pc-substituted pyrrolidine-containing $Y_3N@C_{80}$ dyad **3** decomposes under ambient conditions giving rise to the parent endohedral metallofullerene ($Y_3N@C_{80}$) and no further characterization was possible. It has been demonstrated that fulleropyrrolidine adducts undergo retro-1,3-dipolar cycloadditions under thermal and electrochemically oxidative conditions.[27] The retro-cycloaddition reaction seems to happen even faster in the case of $Y_3N@C_{80}$ derivatives containing with electron donor units, probably due to their marked difference in electronic character.

However, when considering ferrocene carboxaldehyde as precursor of the donor unit in the 1,3-dipolar cycloaddition reaction of azomethine ylides to form $M_3N@C_{80}$-based dyads, the stability of the obtained compounds (**4**[17] and **5**) was found to be quite different from that of compound **3**. After reacting $Y_3N@C_{80}$ with N-methylglycine and ferrocene carboxaldehyde **2**, the formation of multiple adducts was observed. Nonetheless, the major fraction was isolated by using preparative silica gel TLC and found to correspond to the N-methyl-2-ferrocenyl-[6,6]–I_h-$Y_3N@C_{80}$-fulleropyrrolidine (**5**). This dyad exhibits a 9.3 min retention time on a Buckyclutcher column eluting with toluene (4 mL min^{-1}) (see Figure S5). The regioselective 1,3-dipolar cycloaddition reaction at a [6,6] bond was inferred from the irreversible electrochemistry of the isolated adduct (see Electrochemical Section).

The ^{1}H NMR spectrum of compound **5** shows individual resonances for the protons of the cyclopentadienyl (Cp) ring directly attached to the pyrrolidine ring in the region between δ 4.6 and 4.25 ppm (Figure 1b). The geminal protons on the pyrrolidine ring appear as two doublets separated by $\approx$1.2 ppm due to the asymmetry introduced by the ferrocenyl group. One of the doublets ($^1J(H,H) = 9.6$ Hz) overlaps with the singlet originating from the unsubstituted Cp ring at 4.19 ppm; while the other one is observed at 3.0 ppm. The remaining proton in the pyrrolidine ring appears as a singlet at δ 3.63 ppm while the N-methyl group is observed as a singlet at 3.14 ppm. The presence of only one set of signals for the pyrrolidine protons clearly indicates that we only have one pair of enantiomers out of the possible two, or that at least one pair of them was present in a higher proportion and the less abundant pair was not detected by ^{1}H NMR (Figure 1b). No other significant signals were observed, implying that the carbon of the pyrrolidine ring next to the ferrocene unit shows a preference for either the pyrene-like or corannulene-like carbon. There are many examples illustrating the regioselectivity of the 1,3-dipolar cycloaddition reactions over asymmetric olefin substrates (before copper catalysts were developed)[28] in which the attack of the dipole is strongly influenced by steric and electronic factors.[29] Surprisingly, when compound **5** was heated at 150 °C, instead of the expected isomerization of the [6,6] adduct to the [5,6] adduct—as previously observed in similar systems[22]—a retro-cycloaddition reaction to give back I_h-$Y_3N@C_{80}$ was observed. The sensitivity of adduct **5** to light and temperature was also evident in the MALDI-TOF mass spectrum where only the peak corresponding to $Y_3N@C_{80}{}^{+\bullet}$ was ob-
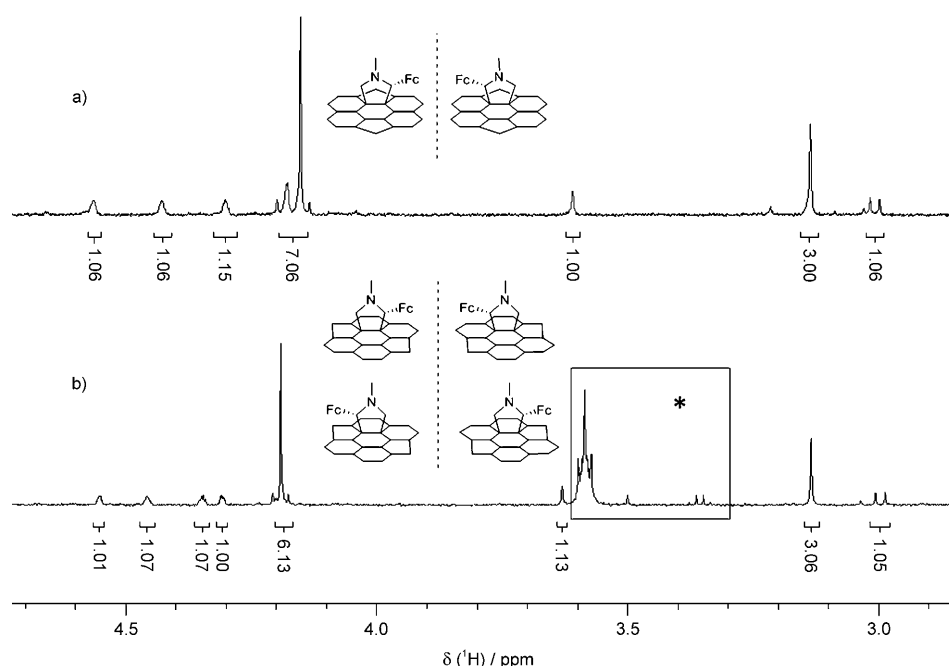
Figure 1. ^{1}H NMR spectra of a) **4** in $CS_2/[D_4]o$-DCB and b) **5** in $CS_2/[D_6]$acetone. The insets show the pair of enantiomers formed by addition of the addend at a [5,6]-junction in a) and the two possible isomers by addition of the addend at a [6,6]-junction in b): the pyrrolidine carbon atom holding the ferrocenyl moiety could be attached to a pyrene-like carbon or to a corannulene-like carbon. * The signal in the box of Figure 1b denotes impurities from the solvent.

served even though 9-nitroanthracene was used as matrix and the analysis was performed in negative ionization mode (Figure S6).[9a]
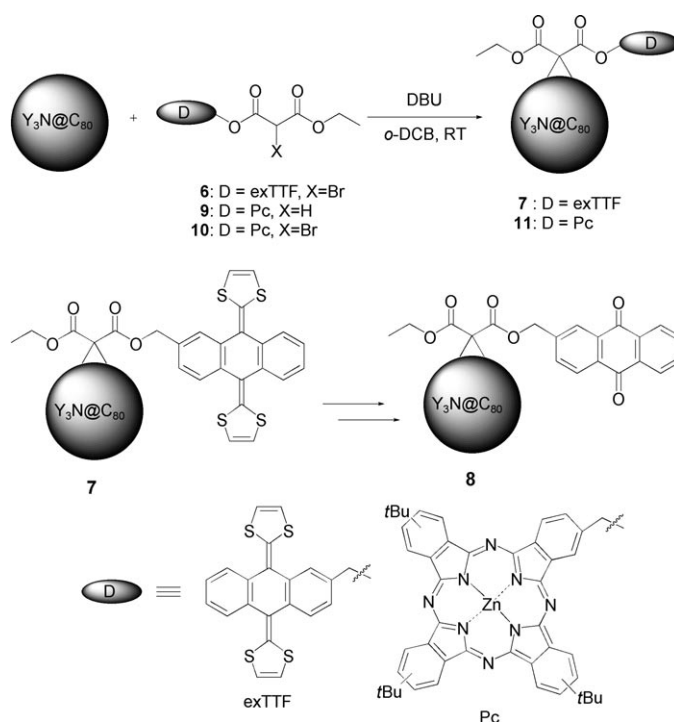
When aldehyde **2** was reacted with I_h-Sc$_3$N@C$_{80}$ in the presence of *N*-methylglycine, adduct **4** was formed. This dyad showed a retention time of 11.53 min on a Bucky-clutcher column (toluene 4 mL min^{-1}) and reversible electrochemistry which suggests that it was the [5,6] regioisomer (see Electrochemical Section).[17] The ^{1}H NMR spectrum of this adduct shows individual resonances for the protons in the Cp ring attached directly to the pyrrolidine in the region from δ 4.60 to 4.25 ppm (Figure 1a). The pyrrolidine geminal protons are separated by ≈ 1.2 ppm and appear as doublets at 4.18 and 3.01 ppm ($J = 9.5$ Hz). The proton on the methine carbon appears at 3.61 ppm, while the *N*-methyl protons appear as a singlet at 3.14 ppm. The coupling between the protons in the Cp ring was evident in the COSY spectrum. By HMQC the carbons with protons attached to them could be assigned. The MALDI-TOF mass spectrum of compound **4** was obtained by using 9-nitroanthracene as matrix and running in negative ionization mode showed the molecular ion peak but also the peak corresponding to the fragment Sc$_3$N@C$_{80}^{+\cdot}$. Dyad **4**, in contrast with the other pyrrolidine-based Y$_3$N@C$_{80}$ (M = Sc, Y) dyads (**3** and **5**) was found to be relatively stable at room temperature for over two months.

In an attempt to prepare other types of TNT endohedral fullerene-based dyads, we decided to test the Bingel–Hirsch reaction on Y$_3$N@C$_{80}$[30] since the corresponding [6,6]-open

di(ethoxycarbonyl)methano adducts withstand thermal as well as reductive/oxidative electrolytic conditions, while I_h-Sc$_3$N@ C$_{80}$ did not react under the same experimental conditions.[11] Taking advantage of the proven stability of the Y$_3$N@C$_{80}$ malonate fulleroids, two dyad systems were prepared by following the Bingel–Hirsch protocol (Scheme 2).

Compound **6**[31] was reacted with Y$_3$N@C$_{80}$ in the presence of 1,8-diazabicyclo[5.4.0]undec-7-ene (DBU) resulting in the formation of the desired exTTF-containing adduct **7** (see Experimental Section for details). Interestingly, the ^{1}H NMR spectrum of compound **7** showed the benzylic protons appearing as two sets of doublets centered at 5.60 ppm ($J \approx 12$ Hz), both of them distorted due to the roofing effect (Figure 2b). The observed splitting pattern is due to: i) the exTTF moiety adopting a "butterfly" conformation in which the 1,3-dithiolene groups are bent out of the plane of the anthracene core, creating two different magnetic envi-

Scheme 2. Synthesis of the Y$_3$N@C$_{80}$ Bingel derivatives **7**, **8** and **11**.

CHEMISTRY
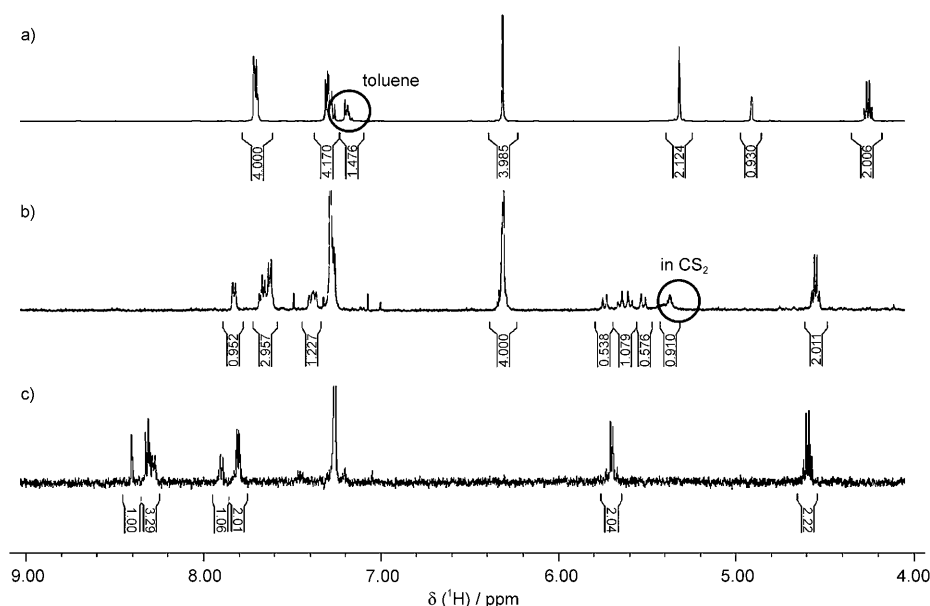**A EUROPEAN JOURNAL**

L. Echegoyen, D. M. Guldi, T. Torres, J. M. Poblet, N. Martín et al.

Figure 2. ^{1}H NMR spectra for a) **6** in CDCl$_3$, b) **7** in CS$_2$/CDCl$_3$ 4:1 and c) **8** in CS$_2$/CDCl$_3$ 4:1. The methyl signals observed at high field are overlapped with grease and solvent impurities and are omitted for clarity. Circle in a) denotes residual toluene after purification and a solvent impurity in b).

ronments for the benzylic protons[31] and, ii) the slow rotation of the exTTF group and the absence of a symmetry plane bisecting the [6,6] bonds of the I_h-Y$_3$N@C$_{80}$ cage which gives rise to two different magnetic environments.

Dyad **7** oxidized spontaneously and was transformed into compound **8** in CHCl$_3$ solution within a few hours, first losing one of the two 1,3-dithiolene groups leading to a very unstable intermediate with a retention time of 18.3 min on HPLC (Figure S7). The loss of the first dithiolene group is followed by the loss of the other 1,3-dithiolene group, ultimately producing the stable adduct **8** containing an anthraquinone moiety. This conclusion is supported by the MALDI-TOF mass spectrum of each individual HPLC fraction collected (Figure S8).

The ^{1}H NMR spectrum of compound **8** shows the benzylic protons as a set of doublets at 5.70 ppm due to hindered rotation of the anthraquinone moiety, confirming the presence of a "butterfly" conformation for the exTTF in the parent compound **7** (Figure 2c). The absence of the vinyl protons signal, added to the fact that all the aromatic signals were downfield compared to those for the parent compound supported our conclusion. The electrochemical characterization further confirmed the structure proposed for adduct **8** (see Electrochemical Section). The decomposition of dyad **7** seems to be the result of a photo-degradation process similar to the one reported for other exTTF analogues,[32] since protecting the sample from light slows down the conversion of **7** into **8**.

For preparation of Pc-based dyad **11**, compound **10** was prepared from tri-*tert*-butylhydroxymethyl-phthalocyaninatozinc(II)[33] **9** (see Experimental Section for details). Compound **10** was reacted with Y$_3$N@C$_{80}$ in the presence of DBU yielding dyad **11**. Unfortunately, compound **11** was

not stable and decomposed in CHCl$_3$ solution under our experimental conditions during the purification process. The formation and degradation of dyad **11** was followed by HPLC as shown in Figure 3. We were able to characterize the two major degradation products, giving insight into the process. One of these was the Y$_3$N@C$_{80}$-monoethylmalonic acid adduct; its MALDI-TOF mass spectrum (Figure 4) resembles the one obtained after treating the Y$_3$N@C$_{80}$-diethylmalonate adduct with metallic sodium,[11a] where the molecular ion peak is not observed because of fragmentation, which gives a peak corresponding to the mass of Y$_3$N@C$_{81}$$^{+\bullet}$, while its HPLC re-
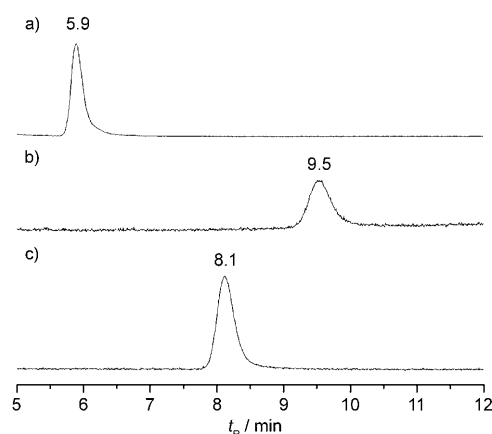

Figure 3. HPLC chromatograms (Buckyclutcher toluene 4 mL min^{-1}) of: a) Y$_3$N@C$_{80}$, b) **11** and, c) Y$_3$N@C$_{80}$ monoethyl malonate adduct obtained by decomposition of dyad **11**.

tention time is very close to that of the Y$_3$N@C$_{80}$-diethylmalonate adduct.[10b] The other decomposition product was the tri-*tert*-butylhydroxymethylphthalocyaninatozinc(II). The two decomposition products of dyad **11** are probably the result of a hydrolysis process. A similar hydrolysis mechanism has recently been proposed by Dorn, Gibson, and co-workers to explain the free radical reaction pathway observed for Sc$_3$N@C$_{80}$-based diethyl malonates when Mn(OAc)$_3$ is used as a catalyst.[14]

In light of the results obtained during the preparation of M$_3$N@C$_{80}$ (M=Sc, Y)-based dyads it seems clear that the well-established methodologies used for the exohedral functionalization of fullerenes do not necessarily apply for endohedral metallofullerenes. Novel synthetic strategies and pu-
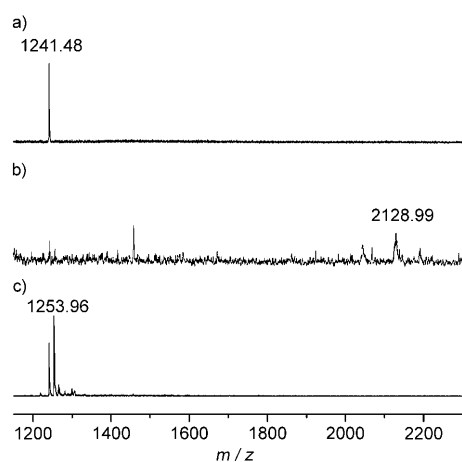
Figure 4. MALDI spectra of: a) $Y_3N@C_{80}$, b) **11** and, c) final monoethylmalonate adduct.

Figure 5. Cyclic voltammograms recorded on a GC electrode (1 mm) in o-DCB containing 0.05 M n-Bu$_4$NPF$_6$ as supporting electrolyte and a scan rate of 100 mV s^{-1} for: a) **7** and b) **8**, * indicates fullerene-based reduction processes.

rification methods need to be explored in order to construct robust dyads based on these endohedral carbon cages.

Electrochemistry: The electrochemical properties of compounds **4**, **5**, **7** and **8** were investigated by cyclic voltammetry at room temperature in o-DCB solutions. Their redox potentials are collected in Tables 1 and 2 (see below), along with those of **2**, exTTF-CHO, and 2-hydroxymethylanthraquinone (AQ-CH$_2$OH), C_{60}, I_h-Sc$_3$N@C$_{80}$, Y_3N@C$_{80}$ and several [5,6] and [6,6]pyrrolidine or metallofullerene adducts of I_h-Sc$_3$N@C$_{80}$, or Y_3N@C$_{80}$ as references.

The I_h-Sc$_3$N@C$_{80}$ and Y_3N@C$_{80}$ cages exhibit irreversible redox processes at a scan rate of 100 mV s^{-1}, although the reductive electrochemistry of I_h-Sc$_3$N@C$_{80}$ becomes reversible at higher scan rates.[34,35] It has also been previously shown that the general electrochemical behavior of M$_3$N@C$_{80}$ derivatives can be employed to differentiate between the two regioisomers formed at [5,6]- and [6,6]-bonds.[22] Reversible electrochemical cathodic behaviors have been observed for [5,6]-monoadducts, whereas the corresponding [6,6]-monoadducts show irreversible behaviors. In line with these considerations, Figure 5 shows representative CVs for the exTTF-based dyad **7**, and the anthraquinone–Y$_3$N@C$_{80}$ Bingel derivative **8**. Dyad **7** exhibits the typical electrochemical behavior of [6,6]-methanofullerene derivatives of Y_3N@C$_{80}$,[22] that is, an irreversible reductive behavior as shown in Figure 5 (trace a). On the oxidation side, the quasi-reversible processes of the respective parent metallofullerene and exTTF[36] are observed at +0.90 and +0.23 V, respectively.

The cyclic voltammogram of anthraquinone–Y$_3$N@C$_{80}$ Bingel adduct **8** shows two reduction and one oxidation waves, corresponding to the reductions of the anthraquinone moiety, and the oxidation of the Y_3N@C$_{80}$ cage, respectively (Figure 5, trace b). The first reduction step at −1.34 V was found to be electrochemically reversible. The second reduction step at −1.72 V and the oxidation step at +0.67 V were found to be electrochemically quasi-reversible by cyclic voltammetry. The shoulders observed at about −1.23 and
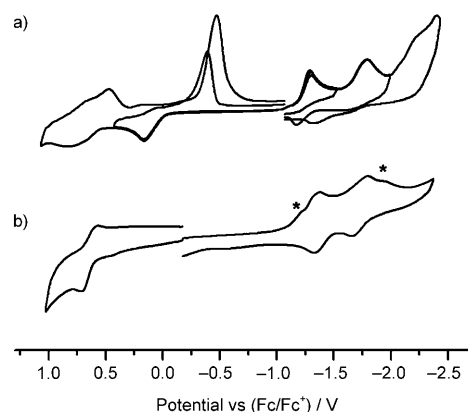
−1.98 V probably correspond to the reduction of the C_{80} cage, since the reductive processes of both fragments (Table 1, entries Y_3N@C$_{80}$ and AQ-CH$_2$OH) occur almost at the same potential. The absence of the oxidation process corresponding to the exTTF addend, and the presence of the two reduction waves of the anthraquinone addend, clearly demonstrated the conversion of exTTF into the anthraquinone adduct of Y_3N@C$_{80}$.

Table 1. Electrochemical reduction potentials [V] vs Fc/Fc$^+$ (o-DCB, 0.05 M nBu$_4$NPF$_6$) of compounds **4**, **5**, **7**, **8** and AQ-CH$_2$OH. Values in brackets indicate peak to peak separation in mV. All values indicate half wave potentials unless indicated. Electrochemical potentials of C_{60}, I_h-Sc$_3$N@C$_{80}$, Y_3N@C$_{80}$, fulleropyrrolidine and methanofullerene adducts of M$_3$N@C$_{80}$ reported previously are included for comparison.[a]

Compound	$E^{0/-}$	$E^{-/2-}$	$E^{2-/3-}$
C_{60}[a]	−1.15	−1.55	−2.01
I_h-Sc$_3$N@C$_{80}$[a]	−1.29	−1.56	−2.32
Y_3N@C$_{80}$[a]	−1.44	−1.83	−2.38
[5,6]-pyrrolidine–I_h-Sc$_3$N@C$_{80}$[a]	−1.18	−1.57	−2.29
[6,6]-pyrrolidine–Y_3N@C$_{80}$[a]	−1.40[b]	−2.04[b]	–
[6,6]-methanofullerene–Y_3N@ C$_{80}$[a]	−1.43[b]	−1.89[b]	–
7	−1.28[b]	−1.77[b]	−2.22[b,c]
8	−1.34(58)[d]	−1.72(117)[d]	–
4	−1.14(66)	−1.53(62)	−2.25(66)
5	−1.41[b]	−1.77[b]	–
AQ-CH$_2$OH	−1.50(128)	−1.84(156)	–

[a] From ref. [22]. [b] Reduction peak potential, irreversible process. [c] Not well defined. [d] Addend based.

The electrochemical reductions of the pyrrolidinofullerene ferrocenyl monoadducts of I_h-Sc$_3$N@C$_{80}$ **4**[17] and I_h-Y$_3$N@C$_{80}$ **5** show different reversibility at a scan rate of 100 mV s^{-1} (Figure 6). This indicates the formation of the different regioisomers: ferrocenyl [6,6]- and [5,6]fulleropyrrolidine of I_h-Y$_3$N@C$_{80}$ and I_h-Sc$_3$N@C$_{80}$, respectively.[22] Three one-electron reversible reductions at −1.14, −1.53, and −2.25 V were observed for the N-methyl-2-ferrocenyl–[5,6]-I_h-Sc$_3$N@

CHEMISTRY
A EUROPEAN JOURNAL

L. Echegoyen, D. M. Guldi, T. Torres, J. M. Poblet, N. Martín et al.

Table 2. Electrochemical oxidation potentials [V] vs Fc/Fc$^+$ (o-DCB, 0.05 M nBu$_4$NPF$_6$) of compounds **2**, **4**, **5**, **7**, **8**, exTTF-CHO. Values in brackets indicate peak to peak separation in mV. All values indicate half wave potentials unless indicated. First oxidation assigned to Sc$_3$N@C$_{80}$, Y$_3$N@C$_{80}$, and fulleropyrrolidine and methanofullerene adducts of M$_3$N@C$_{80}$ reported previously for comparison.[a]

Compound	Addend-based $E^{0/+}$	C$_{80}$-cage-based $E^{0/+}$	$E^{+/2+}$
I_h-Sc$_3$N@C$_{80}$[a]	–	+0.59	–
Y$_3$N@C$_{80}$[a]	–	+0.64	–
[5,6]-pyrrolidine–I_h-Sc$_3$N@C$_{80}$[a]	–	+0.62	–
[6,6]-pyrrolidine–Y$_3$N@C$_{80}$[a]	–	+0.65	–
[6,6]-methanofullerene–Y$_3$N@C$_{80}$[a]	–	+0.60	–
7	+0.23[b]	–	+0.90[c]
8	–	+0.67(131)	–
4	+0.15[b]	+0.61(82)	+1.09(170)
5	+0.07[b]	+0.57(141)	+0.66(96)
2	+0.20(117)	–	–
exTTF-CHO	+0.06[b]	–	–

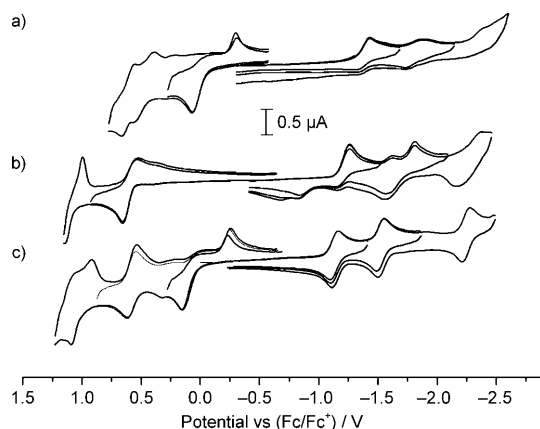[a] From ref. [22]. [b] Oxidation peak potential, irreversible process. [c] Not well defined.

Figure 6. Cyclic voltammograms recorded on a GC electrode (1 mm) in o-DCB containing 0.05 M n-Bu$_4$NPF$_6$ as supporting electrolyte and a scan rate of 100 mV s^{-1} for: a) **5**, b) I_h isomer of Sc$_3$N@C$_{80}$ and, c) **4**.

C$_{80}$-fulleropyrrolidine (**4**) (Figure 6, trace c). Additionally, in the positive potential range three oxidations were observed at +0.15, +0.61, and +1.09 V. The first process at +0.15 V corresponds to the oxidation of the ferrocenyl addend and the processes at +0.61 and +1.09 V are the oxidations of the fullerene cage.

Similar electrochemical behavior was observed for the oxidation of the ferrocenyl addend (+0.07 V) in **5**, since the oxidation of this donor was found to be irreversible by cyclic voltammetry with the re-oxidation shifted about 380 mV in the direction of the negative potential. Two pairs of oxidations were observed for **5** at +0.57 and +0.66 V, one of them can be attributed to the cage-based oxidation of the adduct **5** while the other is possibly a result of electrochemical retrocycloaddition reaction which has been observed in case of pyrrolidino derivatives of Sc$_3$N@C$_{80}$.[27b] In

contrast to the reductive electrochemical behavior of **4**, the reduction processes of **5** are irreversible and, increasing the scan rate from 100 mV s^{-1} to 20 V s^{-1} do not appreciably alter the appearance of the reduction waves. These results perfectly agree with the electrochemical behavior of [6,6]pyrrolidine adducts of Y$_3$N@C$_{80}$.

Theoretical calculations: As previously mentioned, cycloaddition reactions on I_h-Sc$_3$N@C$_{80}$ usually take place regioselectively at a [5,6] ring junction and Bingel–Hirsch type reactions on the I_h-Y$_3$N@C$_{80}$ derivative occur exclusively at a [6,6] ring junction, as recently demonstrated by X-ray crystallography and DFT calculations.[11a,23] Considering these previous results, we have optimized the geometry of the two possible isomers that result from the different orientation of the two dithiolene rings with respect to the C$_{80}$ cage for derivative **7**: the isomer in which the rings are pointing upwards (up) and that in which the rings are pointing downwards (down). From the different orientations that the M$_3$N unit can adopt inside the fullerene cage, we have chosen that with the lowest energy for each endohedral metallofullerene (EMF) as found in a previous theoretical study.[23] For derivative **7**, the two isomers are almost degenerate (within 1 kcal mol^{-1}), the *down* isomer being the most stable (see Figure 7). The optimized structure of derivative **8**, obtained after oxidation of structure **7**, is also shown in Figure 7.
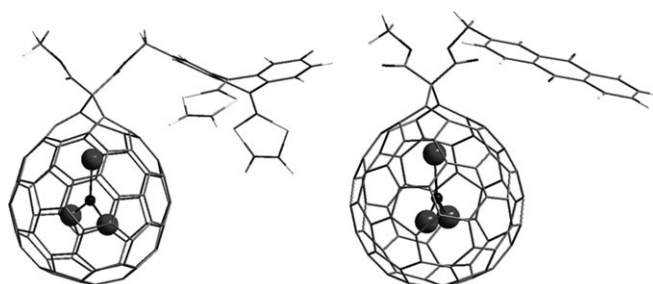

Figure 7. Optimized structures of the down isomer of derivative **7** (left) and the anthraquinone derivative **8** (right).

We have analyzed in detail the electronic structure for the *down* isomer of derivative **7**. As expected by the strong electron donating character of the TTF moiety, the HOMO is localized in this unit whereas the LUMO is localized in the fullerene part of the dyad (Figure S9). In particular, the LUMO is mainly localized in the carbon atoms of the cage being very similar to the LUMO observed for other Y$_3$N@C$_{80}$-fulleropyrrolidino compounds and the parent Y$_3$N@C$_{80}$ cage (Figure S9). The energy of the LUMO in these fullerene systems is actually not very different (within 0.3 eV at our computational level, Table 3). As a consequence, the first reduction peaks in the corresponding CVs should appear at similar reduction potentials as shown experimentally (see Table 1). The triplet state in which one electron is transferred from the donor unit (exTTF) to the acceptor

Table 3. Energy values [eV] for the HOMO and LUMO of structures **4**, **5**, **7**, **8** and reference systems.

Compound	HOMO	LUMO
C_{60}	−6.25	−4.55
I_h-$Sc_3N@C_{80}$	−5.78	−4.59
I_h-$Sc_3N@C_{80}$-[5,6]-pyrrolidine	−5.50	−4.41
4	−4.60	−4.27
I_h-$Y_3N@C_{80}$	−5.92	−4.36
I_h-$Y_3N@C_{80}$-[6,6]-methano adduct	−5.77	−4.26
7	−4.41	−4.08
8	−5.71	−4.21
5	−4.69	−4.14

moiety (metallofullerene), that is, the state with the charge separation, is computed to lay at much higher energies (around 30 kcal mol^{-1}). A plot of the spin density for this triplet state is shown in Figure S10.

For derivative **8**, in contrast to what happens for $Y_3N@C_{80}$−exTTF dyad **7**, the HOMO is localized in the fullerene part because the anthraquinone moiety is not as strong as an electron donor like the TTF derivatives. The LUMO is also localized on the fullerene moiety and it is very similar to the LUMO found in dyad **7**. Indeed, these two LUMOs show very similar energies (Table 3). The LUMO+1, however, is localized on the anthraquinone (Figure S11, top) and is only 0.15 eV less stable than the LUMO. Therefore, it is not straightforward to predict from the energy of the molecular orbitals the localization site of the electron, that is, whether it will be in the anthraquinone moiety or in the carbon cage, once the neutral system has been reduced (see reduction processes for **8** on Figure 5, trace b).

It is important to note that the HOMO–LUMO gaps do not provide the experimental electrochemical gaps obtained from CV, although a correlation exists. The experimental electrochemical gap for dyad **7** is 1.51 V and the computed HOMO–LUMO gap is only 0.33 eV. It is possible, however, to estimate the electrochemical gap from computations (see Experimental Section). The theoretical electrochemical gap for dyad **7** was computed to be 1.47 V, very close to the experimental one.

Finally, we have carried out theoretical studies in order to analyze the relative stability of the different regioisomers and conformers of dyads **4** and **5**, as well as their electronic structures and the nature of their frontier orbitals. As mentioned before, there are two possible isomers when the adduct is formed at a [6,6]-bond: the pyrrolidine carbon atom holding the ferrocenyl moiety can be attached either to a pyrene-like or to a corannulene-like carbon atom of the fullerene (Figure 8). For the [5,6]-regioisomer, however, the pyrrolidine C atom holding the ferrocenyl group can only be attached to corannulene-like C atom of the fullerene, so only one isomer is possible. Furthermore, two possible conformers may exist for each of these isomers.

The two optimized isomers in the $Y_3N@C_{80}$-based dyad are almost degenerate, the pyrene isomer being around 1 kcal mol^{-1} more stable than the corannulene one (Figure 8). We have also computed the energy of the two
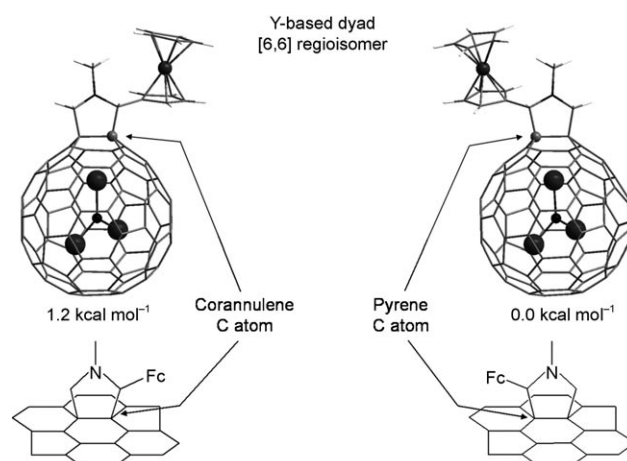

Figure 8. Optimized structures, schematic diagrams and relative energies for the two possible isomers of *N*-methyl-2-ferrocenyl–[6,6]-$Y_3N@C_{80}$-fulleropyrrolidine **5** (corannulene on the left and pyrene on the right).

possible conformations of the ferrocenyl group with respect to the non-planar pyrrolidine ring for both dyads **4** and **5**. The conformer in which the ferrocenyl group is on the same side as the pyrrolidine nitrogen atom, that is, in the equatorial position of the five-membered ring (Figure S12), is more stable than the other conformer, that is, that in which the ferrocenyl group is in the axial position (3.8 kcal mol^{-1} for M=Sc and 6.0 kcal mol^{-1} for M=Y).

The electronic structure of the two dyads was also investigated. As expected by the strong electron-donor character of ferrocene moiety, the HOMO is localized in this unit (Figure 9). HOMO−1 and HOMO−2 are localized on the ferrocenyl moiety as well. The LUMO, however, is localized in the fullerene part of the dyad: for **4**, the LUMO is partially localized in the Sc_3N unit whereas for **5**, the LUMO is delocalized in the carbon atoms of the cage, as observed for dyad **7**.

In order to check the location of the extra electron after reduction, calculations on the monoreduced systems, [*N*-methyl-2-ferrocenyl–I_h-$M_3N@C_{80}$-fulleropyrrolidine]$^-$, (M=Sc, Y), were performed. The spin density is distributed between the M_3N unit and the fullerene cage for M=Sc (Figure S13a) whereas it is fully delocalized in the fullerene framework for M=Y (Figure S13b). The contributions to the total spin density of the different groups that constitute the dyads are collated in Table 4. In particular, 38% of the spin density is located on the Sc_3N unit and 60% in the carbon framework for the Sc-based dyad. For M=Y, however, the extra electron is mostly located on the carbon cage (91%) with a very small contribution to the total spin density from the Y_3N unit (5%).

To further assess the validity of our methodology, the difference in the first reduction potentials of dyads **4** and **5** was computed (see Experimental Section). The predicted value, 260 mV in the gas phase and 225 mV in *o*-DCB solution, agrees well with the experimental value of 200 mV. Howev-
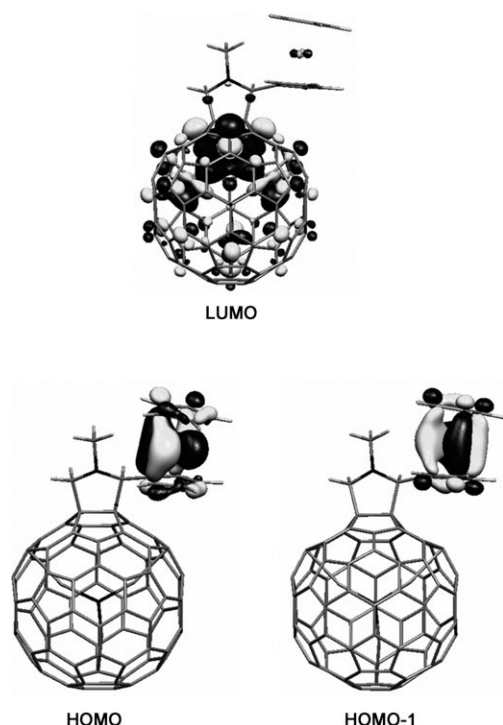
CHEMISTRY
A EUROPEAN JOURNAL

L. Echegoyen, D. M. Guldi, T. Torres, J. M. Poblet, N. Martín et al.

LUMO

HOMO   HOMO−1

Figure 9. Representation of the LUMO (up) and the quasidegenerated HOMO and HOMO−1 (down) of N-methyl-2-ferrocenyl–[5,6]-I_h-Sc$_3$N@C$_{80}$-fulleropyrrolidine **4**.

Table 4. Sum of the atomic spin densities (Mulliken partition) for each of the different groups in the reduced dyads **4** and **5**.

	4	5
M$_3$N	0.383	0.050
pyrrolidine	0.016	0.037
fullerene	0.600	0.911
ferrocene	0.001	0.002

er, we have not been able to compute the electronic structure of the oxidized dyads for **4** and **5** due to the limitations of the mono-reference wavefunctions used in DFT. Multireference methods such as CASSCF or CASPT2 would be required, but the large dimensions of the dyads make them unattainable.

To sum up, the computed HOMO and LUMO energies (Table 3) are able to explain the general trends of the CVs. Dyads **4**, **5** and **7**, with very good electron-donor groups, show higher HOMO energies (around 1 eV) than the pristine M$_3$N@C$_{80}$ EMFs or the functionalized fulleropyrrolidines without these groups. On the other hand, the LUMO energies of the dyads and those of pristine or functionalized EMFs are similar, in good agreement with their analogous topologies. Therefore, the electrochemical gaps for EMF-based dyads are much smaller than for their EMF counterparts. For some dyads, we have checked that the inclusion of some degree of exact exchange in the density functional

yields much larger HOMO–LUMO gaps but provides the same qualitative information.

Photophysical studies: The properties of the excited states of **4** were analyzed by means of different photophysical techniques and compared to those of reference compound I_h-Sc$_3$N@C$_{80}$. In the absorption spectra we see a broad onset in the near-infrared (NIR) region. As a complement to the absorption experiments we turned to fluorescence experiments. I_h-Sc$_3$N@C$_{80}$ exhibits weak fluorescence features—as a kind of mirror image to the ground state absorption—with an apparent maximum at 833 nm. Correspondingly, we derive a singlet excited state energy of 1.5 eV. Attachment of the electron donating ferrocene group leads to a complete quenching of the I_h-Sc$_3$N@C$_{80}$ centered fluorescence. Implicit is a deactivation that involves either electron transfer, energy transfer or heavy ion quenching. It is also interesting that upon photoexciting I_h-Sc$_3$N@C$_{80}$—lacking the electron donating ferrocene—a significant quantity of singlet oxygen (0.55) was found in NIR emission experiments, which was, however, completely abolished in the dyad.

The lack of detectable fluorescence in time-resolved experiments—seen even for I_h-Sc$_3$N@C$_{80}$—led us to probe both compounds in transient absorption measurements. For I_h-Sc$_3$N@C$_{80}$, the following features emerge: maxima at 508/1040 nm and a minimum at 650 nm. These are assigned to the singlet excited state of Sc$_3$N@C$_{80}$. From the corresponding multi-wavelength analyses we derived a surprisingly short singlet excited state lifetime (i.e., 48 ps), typical values found for C$_{60}$ and C$_{60}$ derivatives are on the order of 1.5 ns. Nevertheless, the product of this the fast decay is the corresponding triplet excited state.

We finally turned to time-resolved transient absorption spectroscopy with **4**. Initially we do observe the I_h-Sc$_3$N@C$_{80}$ centered singlet excited state features, which decay quite rapidly. In fact, a singlet excited state lifetime of only 5 ps—a value that is well in line with the close donor–acceptor separation—has been determined for the Fc-substituted I_h-Sc$_3$N@C$_{80}$ **4**. Moreover, the fast decay is associated with marked changes in the differential absorption spectrum. As Figure 10 illustrates, the singlet excited state features (i.e., maxima at 550 and 870 nm) transform over the course of 5 ps into a new set of maxima, which evolve in the visible region (i.e., 530 and 626 nm) as well as in the NIR region (i.e., 830 and 1120 nm).

Radiolytically and spectroelectrochemically generated spectra of the one-electron reduced I_h-Sc$_3$N@C$_{80}$ radical anion (Figure 11) helped in the spectroscopic identification of the photoproduct. Of particular importance is the close resemblance with the photolytically generated spectrum, especially in the NIR part. In the visible portion, features of the one-electron oxidized ferrocenium evolve around 680 nm. Taking this into consideration, we conclude the successful formation of the radical ion pair state. The energy of approximately 1.29 eV has been estimated based on the electrochemically determined redox potentials. In other words, its formation starting from the I_h-Sc$_3$N@C$_{80}$ singlet
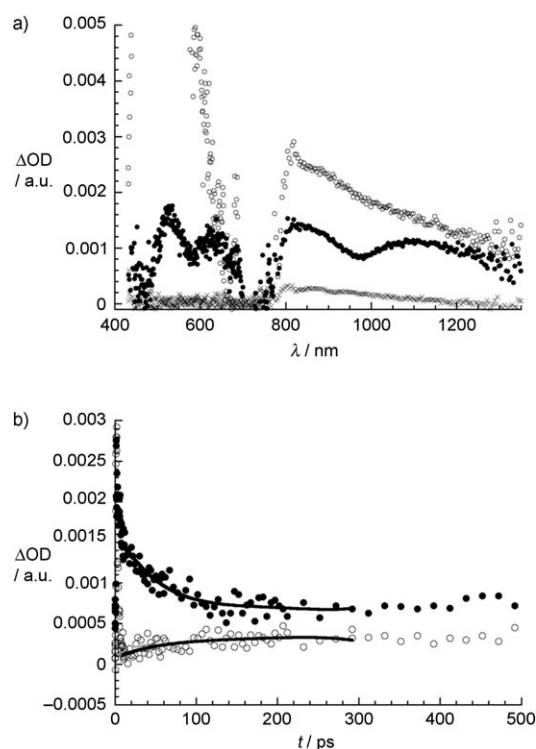
Figure 10. a) Differential absorption spectra (visible and near infrared) obtained upon femtosecond flash photolysis (388 nm, 150 nJ) of **4** in CS_2 with several time delays between 0 and 3000 ps (○: 2 ps, ●: 10 ps, ×: 200 ps) at room temperature. b) Time-absorption profile of the spectra shown above at 625 nm (●) and 1000 nm (○), reflecting the charge separation and charge recombination dynamics.

Figure 11. a) Differential absorption spectrum of I_h-$Sc_3N@C_{80}$ obtained by spectroelectrochemistry in *o*-DCB. b) Differential absorption spectrum following pulse radiolytic reduction of I_h-$Sc_3N@C_{80}$ in a deoxygenated solvent mixture containing toluene, 2-propanol and acetone with $(CH_3)_2$·COH and $(CH_3)_2$·CO$^-$ radicals.

excited state is thermodynamically feasible. The time-absorption profiles in Figure 10b also corroborate that the radical ion pair state is metastable decaying with a lifetime of 128 ps in carbon disulfide and 84 ps in *o*-DCB.

Testing a comparable C_{60} D–A conjugate, that is a ferrocene-based C_{60} dyad, under exactly the same experimental conditions—concentration, solvents and excitation energy—helped to appreciate the impact that using the I_h-$Sc_3N@C_{80}$ exerts on the stabilization of the radical ion pair state.[18] In the tested solvents (i.e., CS_2, THF, and benzonitrile) we see the initially formed C_{60} singlet excited state with a transient maximum at 950 nm rapidly transforming (4.8 ps in THF) into the radical ion pair state. Maxima at 490 and 1010 nm are unequivocal attributes of the one-electron reduced C_{60} moiety, while the general signature of the one-electron oxidized ferrocene is seen around 680 nm. An illustration is provided in Figure S14. The corresponding lifetimes are 46 ps in CS_2, 49 ps in THF and 27 ps in benzonitrile.

Conclusion

We have explored the chemical reactivity of I_h-$Sc_3N@C_{80}$ and I_h-$Y_3N@C_{80}$ to prepare electron transfer model systems with suitable electron-donors, such as tetrathiafulvalene, phthalocyanine, and ferrocene, using 1,3-dipolar cycloaddi-
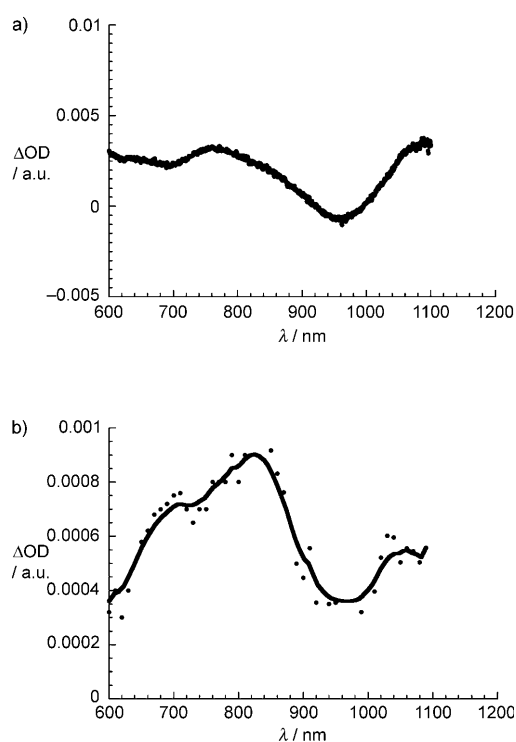
tions of azomethine ylides and Bingel–Hirsch type reactions. The obtained donor–acceptor dyads were shown to have very different stability compared to their C_{60} analogues: The pyrrolidine Pc dyad **3** underwent retro-cycloaddition reaction even at room temperature, the exTTF–Bingel dyad **7** was easily converted to the quinone **8**, whereas for the Pc-based dyad **11**, similarly to the results recently reported by Dorn and co-workers,[14] hydrolysis was also found to be a very favoured process.

By electrochemical means it was shown that the I_h-$Sc_3N@C_{80}$-based dyads contain adducts attached to a [5,6]-double bond ring junction, while the cycloaddition reactions with I_h-$Y_3N@C_{80}$ occur at a double bond at a [6,6]-ring junction. Theoretical calculations confirmed the differences between the redox potentials obtained for the different dyads and provided evidence of the importance of these structures as electron transfer model systems. To confirm this prediction, photophysical investigations were carried out with dyad **4**, where the existence of a photoinduced electron-transfer process was easily detected. Interestingly, for the charged-separated radical ion pair generated after photoexcitation, a lifetime three times longer than that of an equivalent C_{60} dyad was observed.

New synthetic strategies are currently being developed for different, easily accessible, but more stable TNT-based donor–acceptor dyads in order to improve their applicability

CHEMISTRY
A EUROPEAN JOURNAL

L. Echegoyen, D. M. Guldi, T. Torres, J. M. Poblet, N. Martín et al.

and potential performance in solar-energy conversion systems.

Experimental Section

General: Ferrocene carboxaldehyde (**2**) was purchased from Aldrich Chemical Co. Tri-*tert*-butylhydroxymethylphthalocyaninato-zinc(II),[33] tri-*tert*-butyl-(benzaldehyde-4-ethynyl)phthalocyaninatozinc (II) (**1**),[26] 2-(hydroxymethyl)-9,10-bis(1,3-dithiol-2-ylidine)-9,10-dihydro-anthracene,[31] and 9,10-bis(1,3-dithiol-2-ylidine)-9,10-dihydro-2-anthracenyl-hydroxy-methyl-2-bromoethyl malonate[31] were prepared according to published procedures. I_h-Y$_3$N@C$_{80}$ and an isomeric mixture of I_h and D_{5h} Sc$_3$N@C$_{80}$ were provided by Luna Innovations (Nanoworks division). Pure I_h-Sc$_3$N@C$_{80}$ was obtained by eluting a solution of the isomeric mixture through a silica gel column with a plug of tris(4-bromophenyl)aminium-hexachloroantimonate inside, which selectively oxidized the D_{5h} isomer.[34] All reactions were run under an argon atmosphere and followed by TLC on silica plates. Anhydrous solvents were purchased from Aldrich and used as received. NMR spectra were obtained using Bruker Avance 500 or Bruker Avance 300 spectrometers using TMS or residual solvent signals as internal reference. MALDI-TOF mass spectrum was obtained in a Voyager-DE STR mass spectrometer. Preparative TLC was performed using Sorbent silica Gprep w/UV254 500 μm preparative TLC plates. HPLC was performed using a Varian Prostar equipped with a buckyprep-M column and in a Varian Prostar 210 equipped with a bucky-clutcher column.

Theoretical calculations: The calculations were carried out by using DFT methodology with the ADF 2006 program.[37] The exchange-correlation functionals of Becke and Perdew were used.[38] Relativistic corrections were included by means of the ZORA formalism. Triple-ζ polarization basis sets were employed to describe the valence electrons of the C, N, O, S, H, Fe, Sc, and Y atoms. Frozen cores consisting of: i) the 1s shell for C, N, O; ii) the 1s to 2p shells for S, Sc and Fe; and iii) the 1s to 3d shells for Y were described by means of single Slater functions. The calculations for predicting the electrochemical gaps have been done in the presence of a continuous model solvent by means of the conductor-like screening model (COSMO)[39] implemented in the ADF code.[40] To define the cavity that surrounds the molecules we use the solvent excluding surface (SES) method and a fine tesserae. The radii of the atoms, which define the dimensions of the cavity surrounding the molecule, are chosen to be 1.00 Å for Sc and Y, 1.52 for O, 1.55 for N, 1.70 for C, 1.80 for S and 1.20 for H. The dielectric constant is set to 9.8 so as to model *o*-dichlorobenzene as solvent. The electrochemical gap for dyad **7** is computed as the difference between the electron affinity and the ionization potential in *o*-dichlorobenzene solution. On the other side, the difference between the reduction potentials of **4** and **5** are computed as the difference between their electron affinities in *o*-dichlorobenzene solution. In both cases, neither thermal nor entropic effects have been taken into account. This approximation has shown to provide results in agreement with experiments for reduced polyoxometalates in which the extra electrons are delocalized thorough the whole framework similarly to what happens in endohedral metallofullerenes.[41]

Electrochemistry: All electrochemical measurements were performed in *o*-dichlorobenzene (*o*-DCB) with 0.05 M tetra(*n*-butyl)ammonium hexafluorophosphate (*n*Bu$_4$NPF$_6$) as supporting electrolyte. *n*Bu$_4$NPF$_6$ (Aldrich, 98%), was recrystallized three times from ethanol and dried under vacuum for 24 h prior to use. Voltammetric experiments were performed using a potentiostat/galvanostat Model CHI660 A (CH Instruments Electrochemical Workstation) with a three-electrode cell placed in a Faraday cage. The working electrode consisted of a glassy carbon disk (Bioanalytical Systems, Inc.) with a diameter of 1 mm. The surface of the electrode was polished using extra fine carborundum paper (Buehler) followed by 0.3 μm alumina and 0.25 μm diamond polishing compound (Metadi II, Buehler). The electrode was then sonicated in water in order to remove traces of alumina from the metal surface, washed with water, and dried. A silver wire immersed in 0.01 M silver nitrate and 0.05 M *n*Bu$_4$NPF$_6$ in

acetonitrile and separated from the analysis solution by a ceramic tip (Bioanalytical System Inc.) served as the reference electrode. The silver hexafluorophosphate solution was replaced daily, because of the instability of Ag$^+$ to photoreduction. The stability of the reference electrode was examined by recording the ferrocene oxidation potential in the solvent studied as a function of time. The formal potential of the ferrocene/ferrocenium system was found to be stable for about 12 h. The counter electrode was made from platinum mesh (0.25 mm) and was cleaned by heating in a flame for approximately 30 seconds. The solution was deaerated for 20 min with argon prior to the electrochemical measurements. Spectroelectrochemical measurements were taken on a CARY 5000 UV/Vis-NIR spectrophotometer attached to a Princeton Model 263A potentiostat. The experiments were done in *o*-DCB with 0.2 M tetra(*n*-butyl)ammonium perchlorate (*n*Bu$_4$ClO$_4$) as supporting electrolyte employing a three-electrode setup. The working electrode was a platinum mesh with the counter electrode being a platinum plate and silver rod as a reference electrode. The differential spectrum was obtained by subtracting the spectrum taken with applied voltage from the one in the absence of the applied voltage.

Photophysics: Femtosecond transient absorption studies were performed with 530 and 650 nm laser pulses (1 kHz, 150 fs pulse width) from an amplified Ti/Sapphire laser system (Model CPA 2101, Clark-MXR Inc.). Pulse radiolysis experiments were performed using 50 ns pulses of 15 MeV electrons from a linear electron accelerator (LINAC). Dosimetry was based on the oxidation of SCN$^-$ to (SCN)$_2$$^{•-}$ which in aqueous, N$_2$O-saturated solution takes place with G$\approx$6 (G denotes the number of species per 100 eV, or the approximate μM concentration per 10 J absorbed energy). The radical concentration generated per pulse was varied between $(1–3)\times10^{-6}$ M.

Tri-*tert*-butyl(monoethyl ester malonate)phthalocyaninatozinc(II) (9): A flask was charged under argon with CH$_2$Cl$_2$ (6 mL), NEt$_3$ (31.3 mg, 43 μL, 0.31 mmol) and tri-*tert*-butylhydroxymethylphthalocyaninato-zinc(II)[33] (60 mg, 0.08 mmol). The solution was then sonicated for 5 min and a solution of 3-chloro-3-oxopropionate (46.5 mg, 40 μL, 0.31 mmol) in CH$_2$Cl$_2$ (1 mL) added slowly to the solution while stirring. The solution was let to stir at room temperature for 5 h. and then reduced in volume. The crude product was purified by flash column chromatography (SiO$_2$, toluene/EtOAc 3:1) to afford the Pc **9** as a dark-green solid (62 mg, 90%). $R_f = 0.71$ (toluene/EtOAc 3:1); m.p. >300°C; ^{1}H NMR (300 MHz, [D$_6$]DMSO, 25°C, residual solvent): $\delta = 9.4–9.0$ (br, 8H, Ar$_H$), 8.41–8.25 (br, 3H, Ar$_H$), 8.19–7.95 (br, 1H, Ar$_H$), 5.71 (s, 2H; CH$_2$), 4.28–4.12 (m, 2H), 3.82 (s, 2H), 1.78 (s, 27H; *t*Bu), 1.36–1.31 ppm (m, 3H); UV/Vis (CHCl$_3$): $\lambda_{max} = (\log\varepsilon) = 286$ (4.39), 340 (4.59), 609 (4.08), 643 (shoulder) (3.98), 677 nm (4.86); MALDI-TOF MS (for C$_{50}$H$_{48}$N$_8$O$_4$Zn, FW = 890.4; dithranol): m/z (%): 888.3–895.3 (isotopic pattern) (100) [M]$^+$, 1776.6–1786.6 (isotopic pattern) (5) [$2M$]$^+$.

2-Bromo-ethyl-[tri-*tert*-butylhydroxymethylphthalocyaninato-zinc(II)]-malonate (10): A flask was charged under argon with Pc **9** (20 mg, 0.02 mmol), CBr$_4$ (74.5 mg, 0.22 mmol) and CH$_2$Cl$_2$ (5 mL) added. The solution was then cooled down to 0°C for 10 min to while stirring. After this time a solution of DBU (3.0 mg, 3.0 μL) in CH$_2$Cl$_2$ (1 mL) was added slowly to the solution while stirring for 1 h. at 0°C. After this time the solution was let to reach room temperature, diluted with CH$_2$Cl$_2$ (50 mL) and washed with HCl (15 mL, 0.01 N) and brine (2×15 mL). The organic layer was then dried over MgSO$_4$, filtered and reduced in volume to obtain a green powder that was purified by preparative TLC (Merck, silica gel-60, 0.5 mm; toluene/EtOAc 3:1) to obtain the Pc **10** as a green powder (8 mg, 41%). $R_f = 0.82$ (toluene/EtOAc 3:1); m.p. >300°C; ^{1}H NMR (300 MHz, [D$_6$]DMSO, 25°C, residual solvent): $\delta = 9.4–9.0$ (br, 8H, Ar$_H$), 8.41–8.25 (br, 3H, Ar$_H$), 8.19–7.95 (br, 1H, Ar$_H$), 5.73 (s, 2H; CH$_2$), 4.95 (s, 1H; CHBr), 4.28–4.12 (m, 2H), 1.78 (s, 27H; *t*Bu), 1.36–1.31 ppm (m, 3H); UV/Vis (CHCl$_3$): $\lambda_{max}(\log\varepsilon) = 286$ (4.38), 340 (4.56), 609 (4.07), 643 (shoulder) (3.98), 677 nm (4.87); MALDI-TOF MS (C$_{50}$H$_{47}$BrN$_8$O$_4$Zn, FW = 969.3; dithranol): m/z (%): 966.3–975.3 (isotopic pattern) (100) [M]$^+$, 887.4–894.3 (isotopic pattern) (20) [M–Br]$^+$, 1934.3–1944.3 (5) [$2M$]$^+$.

N-Methyl-2-[tri-*tert*-butyl(phenyl-4-ethynyl)phthalocyaninato-zinc(II)]-Y$_3$N@C$_{80}$-fulleropyrrolidine (3): An excess of *N*-methylglycine (1.91 mg,

0.21 mmol, 4.4 equiv) and tri-*tert*-butyl-(benzaldehyde-4-ethynyl)phthalocyaninatozinc (II) (**2**),[26] (35.40 mg, 0.040 mmol, 8.3 fold) were placed in a flask containing dried molecular sieves (1 g, 4 Å) under argon. Then DMF (5 mL) was added and the mixture was stirred for 10 min. Then, a solution of I_h-Y$_3$N@C$_{80}$ (5.91 mg, 0.0048 mmol, 1 equiv) in *o*-DCB (10 mL) was added and the mixture stirred for 30 min at RT. Then, the reaction was heated to 120 °C under argon. The progress of the reaction was followed by TLC and took about 2 h and 25 min to complete. The reaction mixture was then filtered and toluene (75 mL) was added to the filtrate. The resulting solution was extracted with water and brine; the organic layer was dried over Mg$_2$SO$_4$, and the solvent was removed under vacuum. The resulting residue was purified by column chromatography (SiO$_2$, CS$_2$, followed by CS$_2$/CHCl$_3$ 1:1, and then CHCl$_3$/EtOAc 20:1) and monoadduct **5** was obtained (0.5 mg, 5 %) after HPLC purification. HPLC retention time (Buckyprep-M, 1% pyridine/toluene 4 mL min^{-1}) 10.4 min; MALDI-TOF (1,8,9-trihydroxyanthracene): *m/z*: 1241 [Y$_3$N@C$_{80}$], 900 [M^+−Pc−CH(CH$_3$)NCH$_2$]. No further characterization was carried out since compound **3** experiments a fast retro-1,3-dipolar cycloaddition at room temperature.

***N*-Methyl-2-ferrocenyl-[5,6]-I_h-Sc$_3$N@C$_{80}$-fulleropyrrolidine (4):** I_h-Sc$_3$N@C$_{80}$ (2.21 mg, 0.002 mmol, 1 equiv), *N*-methylglycine (2.80 mg, 0.031 mmol, 15 equiv) and ferrocene carboxaldehyde (20.78 mg, 0.097 mmol, 49 equiv) were dissolved in a mixture of anhydrous toluene (10 mL) and anhydrous *o*-DCB (10 mL) in a Schlenk flask equipped with a magnetic stirrer under argon. The mixture was heated and stirred for 45 minutes at 120 °C using an oil bath. The solvent was evaporated under a stream of nitrogen until the volume was approximately 5 mL. The reaction mixture was purified using a silica gel column, first with CS$_2$ in order to recover unreacted I_h-Sc$_3$N@C$_{80}$ which eluted with the solvent front. The column was then eluted with a 1:1 mixture of CS$_2$ and toluene to give the desired product. After evaporation, washing with diethyl ether, and drying of the residual solid a black powder was obtained (1.20 mg, 44 %). HPLC (Buckyclutcher, toluene 5 mL min^{-1}): t_R = 11.3 min; ^{1}H NMR (500 MHz, CS$_2$/[D$_4$]*o*-DCB 3:2, 25 °C, residual solvent): δ = 4.70 (br, 1H), 4.53 (br, 1H), 4.39 (br, 1H), 4.27 (br, 1H), 4.25 (s, 5H; Cp), 4.21 (d, 1H, ^1J(H,H) = 9.5 Hz), 3.65 (s, 1H), 3.01 (d, 1H, ^1J(H,H) = 9.5 Hz), 3.20 ppm (s, 3H; CH$_3$); MALDI-TOF (negative ionization mode 9-nitroanthracene as matrix): *m/z*: 1350.15.

***N*-Methyl-2-ferrocenyl–[6,6]-I_h-Y$_3$N@C$_{80}$-fulleropyrrolidine (5)**: I_h-Y$_3$N@C$_{80}$ (1.17 mg, 0.00094 mmol, 1 equiv), *N*-methylglycine (1.32 mg 0.0149 mmol, 15.8 equiv) and, ferrocene carboxaldehyde (10.4 mg, 0.048 mmol, 51.7 equiv) were poured into a Schlenk flask under argon. Then anhydrous *o*-DCB (10 mL) was added using a syringe. The mixture was heated and stirred magnetically for 2 h at 120 °C using a preheated oil bath and the progress of the reaction was followed by TLC. The solvent was evaporated under a stream of nitrogen to dryness. The reaction mixture was purified using preparative TLC plates, first with CS$_2$ in order to recover the unreacted I_h-Y$_3$N@C$_{80}$ which eluted with the solvent front. The plate was dried and eluted again with a 3:2 mixture of CS$_2$ and toluene to elute the desired product as a black band (R_f = 0.85). After evaporating, washing, and drying of the residual solid with diethyl ether, a black powder was obtained (0.63 mg, 45.2 %). HPLC (Buckyclutcher, toluene 4 mL min^{-1}): t_R = 9.3 min; ^{1}H NMR (500 MHz, CS$_2$/[D$_6$]acetone 9:1, 25 °C, TMS): δ = 4.39 (br, 1H), 4.30 (br, 1H) 4.20 (br, 1H), 4.16 (br, 1H), 4.06 (s, 5H; Cp), 4.05 (d, 1H, ^1J(H,H) = 9.5 Hz), 3.54 (s, 1H), 2.96 (d, 1H, ^1J(H,H) = 9.5 Hz), 3.09 ppm (s, 3H; CH$_3$).

81-[9,10-Bis(1,3-dithiol-2-ylidene)-9,10-dihydro-2-anthracenylmethyloxycarbonyl]-81-(ethoxycarbonyl)-1,2-methano-[6,6]-I_h-Y$_3$N@C$_{80}$]fullerene (7): I_h-Y$_3$N@C$_{80}$ (11.8 mg, 0.0095 mmol, 1 equiv) was placed, along with 9,10-bis(1,3-dithiol-2-ylidene)-9,10-dihydro-2-anthracenylhydroxymethyl 2-bromoethyl malonate[31] (40.1 mg 0.0663 mmol, 3.4 equiv), in a round bottom flask equipped with a magnetic stirrer. The system was dried under vacuum and then filled with argon. 1,2-dichlorobenzene (10 mL) was added and agitation started; then DBU (5 µL, 0.033 µmol) dissolved in CHCl$_3$ (1.0 mL) was added dropwise. After two hours no reaction was observed by TLC. An extra portion of DBU (5 µL) was added dropwise. The progress of the reaction was followed by TLC, eluting first with CS$_2$ to move unreacted I_h-Y$_3$N@C$_{80}$. After drying the plate, it was eluted with

CHCl$_3$. The product was observed eluting almost with the front of the solvent. When a second fraction began to appear, the reaction was stopped. The reaction mixture was then concentrated under vacuum and purified on preparative TLC silica plates. The product was recovered from the silica using CHCl$_3$ and dried to obtain the title compound (1.6 mg, 9.5 %; 13.5 %, based on recovered I_h-Y$_3$N@C$_{80}$). ^{1}H NMR (500 MHz, CS$_2$/CDCl$_3$ 4:1, 25 °C, TMS): δ = 7.82–7.20 (br, 7H), 6.30 (s, 4H), 5.72–5.48 (2d, 1H each one, ^1J(H,H) = 11.8 Hz), 4.52 (q, 2H, ^3J(H,H) = 7.0 Hz; CH$_2$), 1.3 ppm (t, 3H, ^3J(H,H) = 7.0 Hz; CH$_3$); MALDI-TOF (positive mode): *m/z*: 1763.57.

This material was unstable and underwent conversion to **8** (HPLC: t_R = 23.8 min); ^{1}H NMR (500 MHz, CDCl$_3$, 25 °C, TMS): δ = 8.4 (d, 1H, ^4J(H,H) = 1.8 Hz; Ar$_H$), 8.32 (d, 1H, ^3J(H,H) = 8.0 Hz; Ar$_H$), 8.30 (br, 2H; Ar$_H$), 7.90 (dd, 1H, ^4J(H,H) = 1.8 Hz, ^3J(H,H) = 8.0 Hz), 7.8 (br, 2H), 5.71 (d, 1H, ^1J(H,H) = 11.0 Hz) 5.68 (d, 1H, ^1J(H,H) = 11.0 Hz), 4.60 (q, 2H, ^3J(H,H) = 6.6 Hz; CH$_2$), 1.42 ppm (t, 3H, ^3J(H,H) = 6.6 Hz; CH$_3$). MALDI-TOF (positive mode): *m/z*: 1592.17.

81-Ethyl-[tri-*tert*-butylhydroxymethyloxycarbonylphthalocyaninatozinc(II)]-81-(ethoxycarbonyl)-[6,6]-I_h-Y$_3$N@C$_{80}$]fullerene (11): I_h-Y$_3$N@C$_{80}$ (0.82 mg, 0.66 µmol) and 2-bromoethyl [tri-*tert*-butylhydroxymethylphthalocyaninato-zinc(II)] malonate (**10**) (1.60 mg, 1.72 µmol) were poured in a 10 mL Schlenk flask equipped with a magnetic stirrer. The flask was purged of air and then filled with argon. *o*-DCB (3.0 mL) was transferred using a cannula and stirring was started. DBU (1.0 µL) was added by using an HPLC syringe and the reaction mixture was stirred for 4 h. The reaction mixture was purified by preparative TLC. First, the plate was eluted with CS$_2$ in order to remove unreacted I_h-Y$_3$N@C$_{80}$, which elutes with the solvent front. There was a spot with an R_f value of 0.3 corresponding to the I_h-Y$_3$N@C$_{80}$-monoethylmalonic acid adduct [MALDI-TOF (positive mode): *m/z*: 1253.96 (base peak), 1298 M^+ −(CH$_3$CH$_2$−CO$_2$) no molecular peak was observed, this compound has an 8.13 min retention time on HPLC (Buckyclutcher, toluene 4 mL min^{-1})]. The desired product **11** barely moved on the silica plate. By eluting with CH$_2$Cl$_2$ it moved with the solvent front. On HPLC the desired adduct has a t_R = 9.50 min (Buckyclutcher, toluene 4 mL min^{-1}). MALDI-TOF: *m/z*: 2125.81.

[1] a) *Fullerenes: From Synthesis to Optoelectronic Properties* (Eds.: D. M. Guldi, N. Martín), Kluver Academic Publishers, Dordrecht, **2002**; b) *The Chemistry of Fullerenes* (Ed.: A. Hirsch), Wiley-VCH, Weinheim, **2005**; c) *Chemistry of Carbon Nanotubes* (Ed.: V. A. Basiuk), American Scientific Publishers, CA, **2006**; d) *Fullerenes: Principles and Applications* (Eds.: F. Langa de la Puente, J. F. Nierengarten), RSC Nanoscience and Nanotechnology Series, Cambridge, United Kingdom, **2007**.

CHEMISTRY
A EUROPEAN JOURNAL

L. Echegoyen, D. M. Guldi, T. Torres, J. M. Poblet, N. Martín et al.

[2] N. Martín, *Chem. Commun.* **2006**, 2093–2104.

[3] For reviews, see: a) A. Hirsch, *Angew. Chem.* **2002**, *114*, 1933–1939; *Angew. Chem. Int. Ed.* **2002**, *41*, 1853–1859; b) J. L. Barh, J. M. Tour, *J. Mater. Chem.* **2002**, *12*, 1952–1958; c) S. Niyogi, M. A. Hamon, H. Hu, B. Zhao, P. Bhomwik, R. Sen, M. E. Itkis, R. C. Haddon, *Acc. Chem. Res.* **2002**, *35*, 1105–113; d) Y.-P. Sun, K. Fu, Y. Lin, W. Huang, *Acc. Chem. Res.* **2002**, *35*, 1096–1104; e) S. Banerjee, M. G. C. Kahn, S. S. Wong, *Chem. Eur. J.* **2003**, *9*, 1898–1908; f) D. Tasis, N. Tagmatarchis, V. Georgakilas, M. Prato, *Chem. Eur. J.* **2003**, *9*, 4000–4008; g) C. A. Dyke, J. M. Tour, *Chem. Eur. J.* **2004**, *10*, 812–817; h) S. Banerjee, T. Hemraj-Benny, S. S. Wong, *Adv. Mater.* **2005**, *17*, 17–29; i) D. M. Guldi, G. M. A. Rahman, F. Zerbetto, M. Prato, *Acc. Chem. Res.* **2005**, *38*, 871–878; j) D. Tasis, N. Tagmatarchis, A. Bianco, *Chem. Rev.* **2006**, *106*, 1105–1136; k) D. M. Guldi, G. M. A. Rahman, V. Sgobba, C. Ehli, *Chem. Soc. Rev.* **2006**, *35*, 471–487; l) D. M. Guldi, *Phys. Chem. Chem. Phys.* **2007**, *9*, 1400–1420.

[4] J. L. Delgado, M. A. Herranz, N. Martín, *J. Mater. Chem.* **2008**, *18*, 1417–1426.

[5] a) S. Nagase, K. Kobayashi, T. Akasaka, T. Wakahara in *Fullerenes: Chemistry, Physics, and Technology* (Eds.: K. M. Kadish, R. S. Ruoff), John Wiley and Sons, New York, **2000**, pp. 395–436; b) *Endofullerenes: A New Family of Carbon Clusters* (Eds.: T. Akasaka, S. Nagase), Kluwer Academic Publishers, Dordrecht, **2002**.

[6] S. Stevenson, G. Rice, T. Glass, K. Harich, F. Cromer, M. R. Jordan, J. Craft, E. Hajdu, R. Bible, M. M. Olmstead, K. Maitra, A. J. Fisher, A. L. Balch, H. C. Dorn, *Nature* **1999**, *401*, 55–57.

[7] For examples of non-isolated pentagon structures see: a) $Sc_3N@C_{70}$: S. Yang, A. Popov, L. Dunsch, *Angew. Chem.* **2007**, *119*, 1278–1281; *Angew. Chem. Int. Ed.* **2007**, *46*, 1256–1259; b) $DySc_2N@C_{76}$: S. Yang, A. A. Popov, L. Dunsch, *J. Phys. Chem. A* **2007**, *111*, 13659–13663; c) $Tb_3N@C_{84}$: C. M. Beavers, T. Zuo, J. C. Duchamp, K. Harich, H. C. Dorn, M. M. Olmstead, A. L. Balch, *J. Am. Chem. Soc.* **2006**, *128*, 11352–11353; d) $Tm_3N@C_{84}$ and $Gd_3N@C_{84}$: T. Zuo, K. Walker, M. M. Olmstead, F. Melin, B. C. Holloway, L. Echegoyen, H. C. Dorn, M. N. Chaur, C. J. Chancellor, C. M. Beavers, A. L. Balch, A. A. Athans, *Chem. Commun.* **2008**, 1067–1069; or the large cluster families: e) $Tb_3N@C_{88}$: T. Zuo, C. M. Beavers, J. C. Duchamp, A. Campbell, H. C. Dorn, M. M. Olmstead, A. L. Balch, *J. Am. Chem. Soc.* **2007**, *129*, 2035–2043; f) $Nd_3N@C_{88}$: F. Melin, M. N. Chaur, S. Engmann, B. Elliott, A. Kumbhar, A. J. Athans, L. Echegoyen, *Angew. Chem.* **2007**, *119*, 9190–9193; *Angew. Chem. Int. Ed.* **2007**, *46*, 9032–9035; g) $Gd_3N@C_{88}$: M. N. Chaur, F. Melin, B. Elliott, A. J. Athans, K. Walker, B. C. Holloway, L. Echegoyen, *J. Am. Chem. Soc.* **2007**, *129*, 14826–14829.

[8] L. Dunsch, S. Yang, *Small* **2007**, *3*, 1298–1320.

[9] a) E. B. Iezzi, J. C. Duchamp, K. Harich, T. E. Glass, H. M. Lee, M. M. Olmstead, A. L. Balch, H. C. Dorn, *J. Am. Chem. Soc.* **2002**, *124*, 524–525; b) H. M. Lee, M. M. Olmstead, E. Iezzi, J. C. Duchamp, H. C. Dorn, A. L. Balch, *J. Am. Chem. Soc.* **2002**, *124*, 3494–3495; c) Z. Ge, J. C. Duchamp, T. Cai, H. W. Gibson, H. C. Dorn, *J. Am. Chem. Soc.* **2005**, *127*, 16292–16298; d) T. Cai, L. Xu, M. R. Anderson, Z. Ge, T. Zuo, X. Wang, M. M. Olmstead, A. L. Balch, H. W. Gibson, H. C. Dorn, *J. Am. Chem. Soc.* **2006**, *128*, 8581–8589.

[10] a) C. M. Cardona, A. Kitaygorodskiy, A. Ortiz, M. A. Herranz, L. Echegoyen, *J. Org. Chem.* **2005**, *70*, 5092–5097; b) C. M. Cardona, A. Kitaygorodskiy, L. Echegoyen, *J. Am. Chem. Soc.* **2005**, *127*, 10448–10453; c) T. Cai, Z. Ge, E. B. Lezzi, T. E. Glass, K. Harich, H. W. Gibson, H. C. Dorn, *Chem. Commun.* **2005**, 3594–3596; d) L. Echegoyen, C. J. Chancellor, C. M. Cardona, B. Elliott, J. Rivera, M. M. Olmstead, A. L. Balch, *Chem. Commun.* **2006**, 2653–2655; e) T. Cai, C. Slebodnick, L. Xu, K. Harich, T. E. Glass, C. Chancellor, J. C. Fettinger, M. M. Olmstead, A. L. Balch, H. W. Gibson, H. C. Dorn, *J. Am. Chem. Soc.* **2006**, *128*, 6486–6492; f) T. Cai, L. Xu, H. W. Gibson, H. C. Dorn, C. J. Chancellor, M. M. Olmstead, A. L. Balch, *J. Am. Chem. Soc.* **2007**, *129*, 10795–10800.

[11] a) O. Lukoyanova, C. M. Cardona, J. Rivera, L. Z. Lugo-Morales, C. J. Chancellor, M. M. Olmstead, A. Rodríguez-Fortea, J. M. Poblet, A. L. Balch, L. Echegoyen, *J. Am. Chem. Soc.* **2007**, *129*, 10423–10430; b) T. Cai, L. Xu, C. Shu, H. A. Champion, J. E. Reid, C. Anklin, M. R. Anderson, H. W. Gibson, H. C. Dorn, *J. Am. Chem. Soc.* **2008**, *130*, 2136–2137.

[12] a) Y. Iiduka, O. Ikenaga, A. Sakuraba, T. Wakahara, T. Tsuchiya, Y. Maeda, T. Nakahodo, T. Akasaka, M. Kako, N. Mizorogi, S. Nagase, *J. Am. Chem. Soc.* **2005**, *127*, 9956–9957; b) T. Wakahara, Y. Liduka, O. Ikenaga, T. Nakahodo, A. Sakuraba, T. Tsuchiya, Y. Maeda, M. Kako, T. Akasaka, K. Yoza, E. Horn, N. Mizorogi, S. Nagase, *J. Am. Chem. Soc.* **2006**, *128*, 9919–9925.

[13] N. B. Shustova, A. A. Popov, M. A. Mackey, C. E. Coumbe, J. P. Phillips, S. Stevenson, S. H. Strauss, O. V. Boltalina, *J. Am. Chem. Soc.* **2007**, *129*, 11676–11677.

[14] C. Shu, T. Cai, L. Xu, T. Zuo, J. Reid, K. Harich, H. C. Dorn, H. W. Gibson, *J. Am. Chem. Soc.* **2007**, *129*, 15710–15717.

[15] a) D. Gust, T. A. Moore, *Acc. Chem. Res.* **2001**, *34*, 40–48; b) M. R. Wasielewski, *J. Org. Chem.* **2006**, *71*, 5051–5066; c) D. M. Guldi, *Phys. Chem. Chem. Phys.* **2007**, *9*, 1400–1420.

[16] a) N. Martín, L. Sánchez, B. M. Illescas, I. Pérez, *Chem. Rev.* **1998**, *98*, 2527–2548; b) D. M. Guldi, *Chem. Commun.* **2000**, 321–327; c) H. Imahori, *J. Phys. Chem. B* **2004**, *108*, 6130–6143; d) J. L. Segura, N. Martín, D. M. Guldi, *Chem. Soc. Rev.* **2005**, *34*, 31–47; e) N. Martín, L. Sánchez, M. A. Herranz, B. Illescas, D. M. Guldi, *Acc. Chem. Res.* **2007**, *40*, 1015–1024.

[17] For preliminary results on a I_h-$Sc_3N@C_{80}$–ferrocene dyad, please see: J. R. Pinzón, M. E. Plonska-Brzezinska, C. M. Cardona, A. J. Athans, S. S. Gayathri, D. M. Guldi, M. A. Herranz, N. Martín, T. Torres, L. Echegoyen, *Angew. Chem.* **2008**, *120*, 4241–4244; *Angew. Chem. Int. Ed.* **2008**, *41*, 4173–4176.

[18] For covalently linked C_{60}–ferrocene dyads, please see: D. M. Guldi, M. Maggini, G. Scorrano, M. Prato, *J. Am. Chem. Soc.* **1997**, *119*, 974–980.

[19] For very recent examples considering donor–acceptor nanoconjugates with exTTFs, see: a) G. Fernández, E. M. Pérez, L. Sánchez, N. Martín, *Angew. Chem.* **2008**, *120*, 1110–1113; *Angew. Chem. Int. Ed.* **2008**, *47*, 1094–1097; b) M. A. Herranz, C. Ehli, S. Campidelli, M. Gutiérrez, G. L. Hug, K. Ohkubo, S. Fukuzumi, M. Prato, N. Martín, D. M. Guldi, *J. Am. Chem. Soc.* **2008**, *130*, 66–73; c) G. Fernández, E. M. Pérez, L. Sánchez, N. Martín, *J. Am. Chem. Soc.* **2008**, *130*, 2410–2411.

[20] a) G. de la Torre, P. Vázquez, F. Agulló-López, T. Torres, *Chem. Rev.* **2004**, *104*, 3723–3750; b) G. de la Torre, C. G. Claessens, T. Torres, *Chem. Commun.* **2007**, 2000–2015.

[21] N. Tagmatarchis, M. Prato, *Synlett* **2003**, 768–779.

[22] C. M. Cardona, B. Elliott, L. Echegoyen, *J. Am. Chem. Soc.* **2006**, *128*, 6480–6485.

[23] A. Rodríguez-Fortea, J. M. Campanera, C. M. Cardona, L. Echegoyen, J. M. Poblet, *Angew. Chem.* **2006**, *118*, 8356–8360; *Angew. Chem. Int. Ed.* **2006**, *45*, 8176–8180.

[24] a) D. Zhou, H. Tan, C. Luo, L. Gan, C. Huang, J. Pan, M. Liib, Y Wu, *Tetrahedron Lett.* **1995**, *36*, 9169–9172; b) L. Gan, D. Zhou, C. Luo, H. Tan, C. Huang, M. Lu, J. Pan, Y. Wu, *J. Org. Chem.* **1996**, *61*, 1954–1961.

[25] X. Lu, X. He, L. Feng, Z. Shi, Z. Gu, *Tetrahedron* **2004**, *60*, 3713–3716.

[26] G. Bottari, D. Olea, C. Gómez-Navarro, F. Zamora, J. Gómez-Herrero, T. Torres, *Angew. Chem.* **2008**, *120*, 2056–2061; *Angew. Chem. Int. Ed.* **2008**, *47*, 2026–2031.

[27] a) N. Martín, M. Altable, S. Filippone, A. Martín-Domenech, L. Echegoyen, C. M. Cardona, *Angew. Chem.* **2006**, *118*, 1467–1470; *Angew. Chem. Int. Ed.* **2006**, *45*, 110–114; b) O. Lukoyanova, C. M. Cardona, M. Altable, S. Filippone, A. Martín Domenech, N. Martín, L. Echegoyen, *Angew. Chem.* **2006**, *118*, 7590–7593; *Angew. Chem. Int. Ed.* **2006**, *45*, 7430–7433.

[28] V. Rostovtsev, L. Green, V. Fokin, K. Sharpless, *Angew. Chem.* **2002**, *114*, 2708–2711; *Angew. Chem. Int. Ed.* **2002**, *41*, 2596–2599.

[29] a) C. Di Valentin, M. Freccero, R. Gandolfi, A. Rastelli, *J. Org. Chem.* **2000**, *65*, 6112–6120; b) R. J. Heusgen, *J. Org. Chem.* **1968**, *33*, 2291–2297; c) R. Huisgen, *J. Org. Chem.* **1976**, *41*, 403–419.

[30] a) C. Bingel, *Chem. Ber.* **1993**, *126*, 1957–1959; b) A. Hirsch, I. Lamparth, H. R. Karfunkel, *Angew. Chem.* **1994**, *106*, 453–455; *Angew. Chem. Int. Ed. Engl.* **1994**, *33*, 437–438.

[31] S. González, N. Martín, D. M. Guldi, *J. Org. Chem.* **2003**, *68*, 779–791.

[32] A. E. Jones, C. A. Christensen, D. F. Perepichka, A. S. Batsanov, A. Beeby, P. J. Low, M. R. Bryce, A. W. Parker, *Chem. Eur. J.* **2001**, *7*, 973–978.

[33] D. M. Guldi, A. Gouloumis, P. Vázquez, T. Torres, V. Georgakilas, M. Prato, *J. Am. Chem. Soc.* **2005**, *127*, 5811–5813.

[34] B. Elliott, L. Yu, L. Echegoyen, *J. Am. Chem. Soc.* **2005**, *127*, 10885–10888.

[35] M. Krause, L. Dunsch, *ChemPhysChem* **2004**, *5*, 1445–1449.

[36] M. A. Herranz, L. Yu, N. Martín, L. Echegoyen, *J. Org. Chem.* **2003**, *68*, 8379–8385.

[37] a) ADF 2006.01, Department of Theoretical Chemistry, Vrije Universiteit, Amsterdam; b) G. T. te Velde, F. M. Bickelhaupt, E. J. Baerends, C. F. Guerra, S. J. A. Van Gisbergen, J. G. Snijders, T. Ziegler, *J. Comput. Chem.* **2001**, *22*, 931–967.

[38] a) A. D. Becke, *Phys. Rev. A* **1988**, *38*, 3098–3100; b) J. P. Perdew, *Phys. Rev. B* **1986**, *33*, 8822–8824.

[39] a) J. Andzelm, C. Kolmel, A. Klamt *J. Chem. Phys.* **1995**, 103, 9312–9320; b) A. Klamt, G. Schuurmann, *J. Chem. Soc. Perkin Trans. 2* **1993**, 799–805.

[40] C. C. Pye, T. Ziegler, *Theor. Chem. Acc.* **1999**, *101*, 396–408.

[41] J. A. Fernandez, X. Lopez, C. Bo, C. De Graaf, E. J. Baerends, J. M. Poblet, *J. Am. Chem. Soc.* **2007**, *129*, 12244–12253.